IOP Publishing Superconductor Science and Technology
Supercond. Sci. Technol. 29 (2016) 124004 (9pp) doi:10.1088/0953-2048/29/12/124004

Flux jump-assisted pulsed field magnetisation of high-J_c bulk high-temperature superconductors

M D Ainslie[1], D Zhou[1], H Fujishiro[2], K Takahashi[2], Y-H Shi[1] and J H Durrell[1]

[1] Bulk Superconductivity Group, Department of Engineering, University of Cambridge, Trumpington Street, Cambridge CB2 1PZ, UK
[2] Department of Physical Science and Materials Engineering, Faculty of Science and Engineering, Iwate University, 4-3-5 Ueda, Morioka 020-8551, Japan

E-mail: mda36@cam.ac.uk

Received 15 August 2016, revised 12 September 2016
Accepted for publication 28 September 2016
Published 21 October 2016

Abstract

Investigating, predicting and optimising practical magnetisation techniques for charging bulk superconductors is a crucial prerequisite to their use as high performance 'psuedo' permanent magnets. The leading technique for such magnetisation is the pulsed field magnetisation (PFM) technique, in which a large magnetic field is applied via an external magnetic field pulse of duration of the order of milliseconds. Recently 'giant field leaps' have been observed during charging by PFM: this effect greatly aids magnetisation as flux jumps occur in the superconductor leading to magnetic flux suddenly intruding into the centre of the superconductor. This results in a large increase in the measured trapped field at the centre of the top surface of the bulk sample and full magnetisation. Due to the complex nature of the magnetic flux dynamics during the PFM process, simple analytical methods, such as those based on the Bean critical state model, are not applicable. Consequently, in order to successfully model this process, a multi-physical numerical model is required, including both electromagnetic and thermal considerations over short time scales. In this paper, we show that a standard numerical modelling technique, based on a 2D axisymmetric finite-element model implementing the $\boldsymbol{H}$-formulation, can model this behaviour. In order to reproduce the observed behaviour in our model all that is required is the insertion of a bulk sample of high critical current density, J_c. We further explore the consequences of this observation by examining the applicability of the model to a range of previously reported experimental results. Our key conclusion is that the 'giant field leaps' reported by Weinstein *et al* and others need no new physical explanation in terms of the behaviour of bulk superconductors: it is clear the 'giant field leap' or flux jump-assisted magnetisation of bulk superconductors will be a key enabling technology for practical applications.

Keywords: bulk superconductors, trapped field magnets, numerical modelling, pulsed field magnetisation, flux jumps, finite element method (FEM) modelling

(Some figures may appear in colour only in the online journal)

1. Introduction

Large, single grain (RE)BCO (where RE = rare earth or Y) bulk superconductors, acting as trapped field magnets (TFMs), are able to trap magnetic fields greater than 17 T [1, 2], an order of magnitude higher than the maximum field produced by conventional permanent magnets. Such bulk superconductors can exhibit critical current densities, J_cs, of 50 kA cm^{-2} at 1 T and 77 K, resulting in trapped fields of up to 1–1.5 T for standard Y–Ba–Cu–O (YBCO) and greater

than 2 T for (RE)BCO materials [3], with 3 T the highest trapped field at 77 K so far in a 65 mm diameter Gd–Ba–Cu–O (GdBCO) sample [4]. Additionally, neutron-irradiated YBCO samples, fabricated by the so-called U/n method [5, 6], containing improved broken-columnar pinning centres, have exhibited much higher J_cs (up to several hundreds of kA cm^{-2} [5]) and trapped fields greater than 2 T at 77 K with smaller samples only 20 mm in diameter [7].

Investigating and predicting the magnetisation of these materials and developing practical magnetising techniques is crucial to using them as TFMs in a number of engineering applications, such as electrical machines [8–11], magnetic separation [12], magnetic resonance imaging, nuclear magnetic resonance [13–15], and magnetic drug delivery systems [16, 17]. The current, best-known method for magnetising bulk superconductors in practical applications is the pulsed field magnetisation (PFM) technique, whereby a large magnetic field is applied via a pulse on the order of milliseconds; however, a significant issue with existing PFM techniques is that the trapped field is generally much less than that achieved in comparison to slower field cooling (FC) and zero field cooling (ZFC) magnetisation techniques, which themselves need a large magnetising coil/fixture, and hence impractical for practical applications. The world record using PFM, using a modified multi-pulse, stepwise-cooling technique, is only 5.2 T at 29 K [18], which is much less than the true capability of these materials as indicated above. It should be noted that at higher operating temperatures (closer to T_c, such as 77 K), fields have been trapped close to that of FC [7, 19–22].

So-called 'giant field leaps' have been observed by a number of research groups investigating PFM [7, 18, 23–26], and more recently in unpublished experiments carried out in our own research group, where flux jumps occur in the superconductor, and magnetic flux suddenly intrudes into the centre of the superconductor, resulting in a large increase in the measured trapped field at the centre of the top surface of the bulk sample and full magnetisation. Due to the complex nature of the magnetic flux dynamics during the PFM process, simple analytical methods, such as those based on the Bean critical state model (CSM), for example, are not applicable [7, 27], and a multi-physical numerical model is required to include both electromagnetic and thermal considerations over a very short time scale [3]. To date, this 'giant field leap' effect observed in a number of experiments has not yet been conclusively explained and no numerical models have reproduced it.

In this paper, it is shown that this effect can be qualitatively reproduced using a standard numerical modelling technique, based on a 2D axisymmetric finite-element model implementing the $\boldsymbol{H}$-formulation. This numerical model is based on previous models published by the authors, with a modified E–J power law characteristic, representing the normal state resistivity of the superconductor when $J > J_c$. By simply inserting a bulk sample of high J_c, as found in high quality standard samples and neutron-irradiated ones, such 'giant field leaps' or flux jumps are observed in the model, without the need for any new physics to explain the physical mechanism underlying the effect. The magnetic flux dynamics in high J_c samples, compared with normal and low J_c samples, are examined using the numerical modelling results, which have important implications for magnetising bulk superconductors with high trapped fields in practical technological applications.

2. Numerical modelling

2.1. Modelling framework

The numerical model used in this paper is based on the 2D axisymmetric $\boldsymbol{H}$-formulation presented in [26] for a solenoid coil magnetising fixture without a soft iron yoke, implemented using the commercial FEM software package COMSOL Multiphysics 5.2a [28]. The general form, partial differential equation interface of COMSOL is used for the electromagnetic analysis, and the heat transfer module is used for the thermal analysis, which are coupled together as described in [26, 29].

In the 2D axisymmetric $\boldsymbol{H}$-formulation, the governing equations are derived from Maxwell's equations—namely, Faraday's (1) and Ampere's (2) laws:

$$\nabla \times E + \frac{\mathrm{d}\boldsymbol{B}}{\mathrm{d}t} = \nabla \times \boldsymbol{E} + \frac{\mathrm{d}(\mu_0 \mu_r \boldsymbol{H})}{\mathrm{d}t} = 0, \tag{1}$$

$$\nabla \times \boldsymbol{H} = \boldsymbol{J}, \tag{2}$$

where $\boldsymbol{H} = [H_r, H_z]$ represents the magnetic field components, $\boldsymbol{J} = [J_\phi]$ represents the current density and $\boldsymbol{E} = [E_\phi]$ represents the electric field. μ_0 is the permeability of free space, and the relative permeability, μ_r, is 1 for the materials modelled. The electrical properties of the superconductor are modelled using an E–J power law relation [30, 31], $E \alpha J^n$, where $n = 20$ and is a reasonable approximation of Bean's critical state model, for which $n \to \infty$ [3]. However, one addition to the modelling framework in this respect is the inclusion of a normal-state resistivity when the current density in the superconductor is larger than the critical current density, J_c. A modified E–J power law relationship is used, as described in [32–34] and in the FC magnetisation model for bulk MgB_2 presented in [35]. Hence, the resistivity tends towards the normal state resistivity (here ρ_{normal} is assumed to be 3.5×10^{-6} Ωm) when $J > 2$–$2.5J_c$ with $n = 20$ [34]. This gives a more reasonable value for the resistivity than the standard E–J assumption in such situations, where the normalised current density, J/J_c, can be much larger than 1 during the PFM process [36]. Figure 1 shows a comparison of the resistivity, ρ, and electric field, E, for the standard and modified E–J power law relations, where $J_c = 2 \times 10^9$ A m^{-2} is assumed, based on the J_c value of the bulk at 40 K (see figure 2). Figure 1(b) also includes the different regimes of the E–J curve, corresponding to thermally assisted flux flow, flux creep and flux flow [37]. It allows us to discern whether this is a cause of the flux jumps, but also improves the convergence properties of the numerical model.

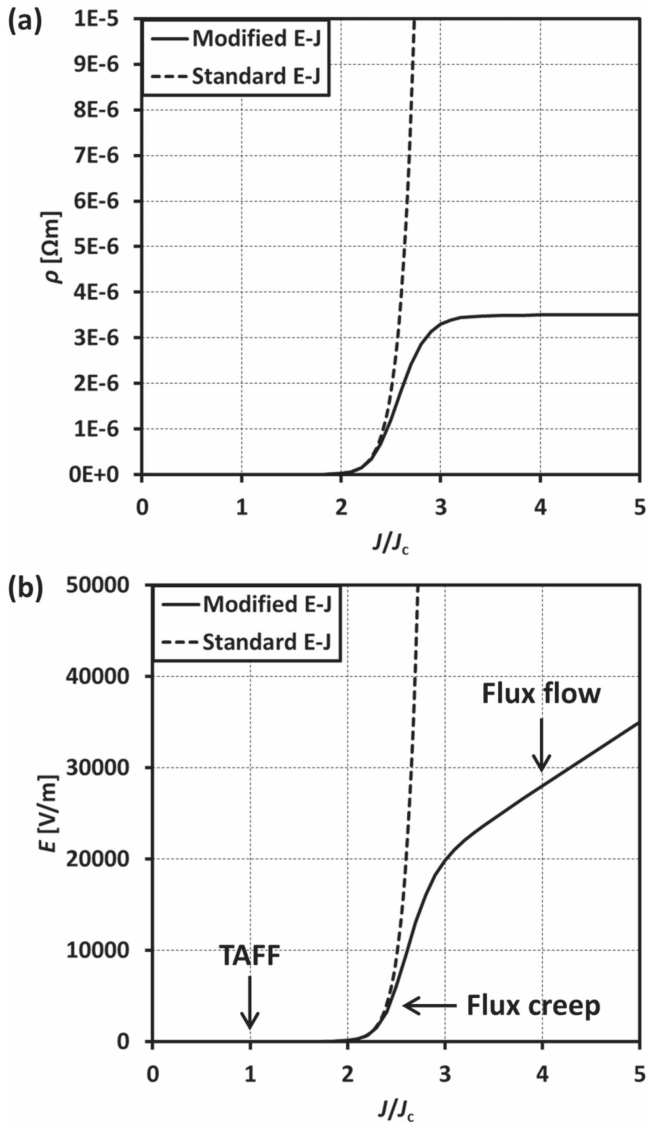

Figure 1. Comparison of (a) resistivity, ρ, and (b) electric field, E, for the standard E–J power law relation, $E \propto J^n$, and the modified E–J power law, where the resistivity tends towards the normal state resistivity when $J > 2$–$2.5J_c$. It is assumed that $n = 20$ and $\rho_{normal} = 3.5 \times 10^{-6}\ \Omega$m.

The results of the numerical model strongly depend on the $J_c(B, T)$ characteristics of the superconductor [3], and the experimental data for $J_c(B)$, measured between 40–85 K from a specimen taken from a representative bulk (15 wt% Ag-containing GdBCO) is input into the model using a two-variable, direct interpolation, as described in [26, 38, 39]. In [26], this experimental data (up to 4 T) was fit up to 10 T using the equation presented in [40] for samples exhibiting a fishtail shape in their magnetisation loop, and these $J_c(B, T)$ characteristics are shown in figure 2. This method of data input is simple and direct, and can significantly improve the computational speed of the model [38, 39]. The 2D axisymmetric model assumes a homogeneous J_c distribution around the *ab*-plane, neglecting any effects from any inhomogeneity of J_c, e.g., [29, 41–43].

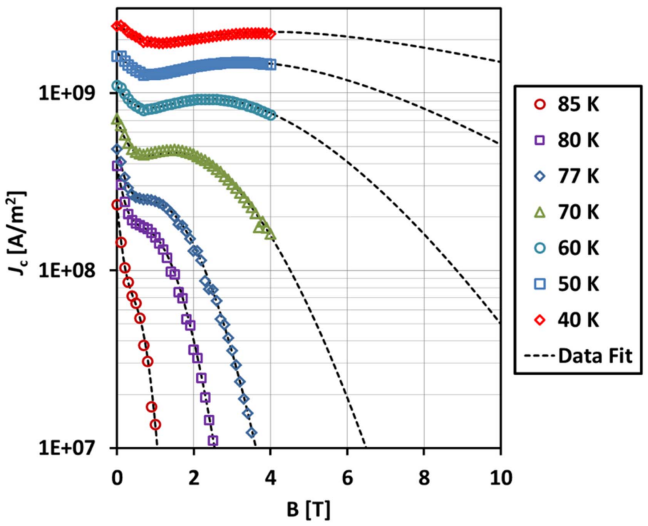

Figure 2. Experimental data for $J_c(B)$, measured from a small sample taken from a representative bulk sample (15 wt% Ag-containing Gd–Ba–Cu–O) [26]. The experimental data is fit up to 10 T using the equation presented in [40] for samples exhibiting a fishtail shape in their $J_c(B)$ curves.

Figure 3 shows the 2D axisymmetric model setup for the numerical simulation. The geometry of the bulk sample is assumed to be 20 mm in diameter and 10 mm thickness, and as a representative magnetising fixture, the solenoid coil experimental setup presented in [26, 29] is used, with the soft iron yoke embedded in the magnetising fixture omitted for simplicity. T_{op} is the operating temperature of the cold head, and is assumed to be 40 K in the following simulations.

Since the temperature of the superconductor can change significantly during PFM [3], the electromagnetic model is coupled with a thermal model, and the thermal behaviour is modelled using the following thermal transient equation:

$$\rho \cdot C\frac{\mathrm{d}T}{\mathrm{d}t} = \nabla \cdot (k\nabla T) + Q. \tag{3}$$

The heat source, Q, in the thermal model is calculated from the product of the electric field and current density throughout the sample, $Q = E_\phi \cdot J_\phi$.

The sample is assumed to be mounted in a 316 stainless steel (SUS) sample holder with Stycast™ 2850 GT, and a thin sheet of indium, approximately 0.2 mm thick, is placed between the cold stage and the sample to ensure a good thermal contact [26]. The thermal properties (thermal conductivity and specific heat) of each of these materials, based on measured experimental data over the temperate range 0–100 K, is input into the model using a linear interpolation function [26, 35]. The indium sheet has a fixed, finite thermal conductivity of 0.5 $\mathrm{Wm^{-1}\,K^{-1}}$ to represent the finite cooling power of the refrigerator and the thermal contact between the cold stage and the bulk, as described in [44].

Pulsed currents of varying magnitude are applied to the solenoid coil via an integral constraint on the copper coil

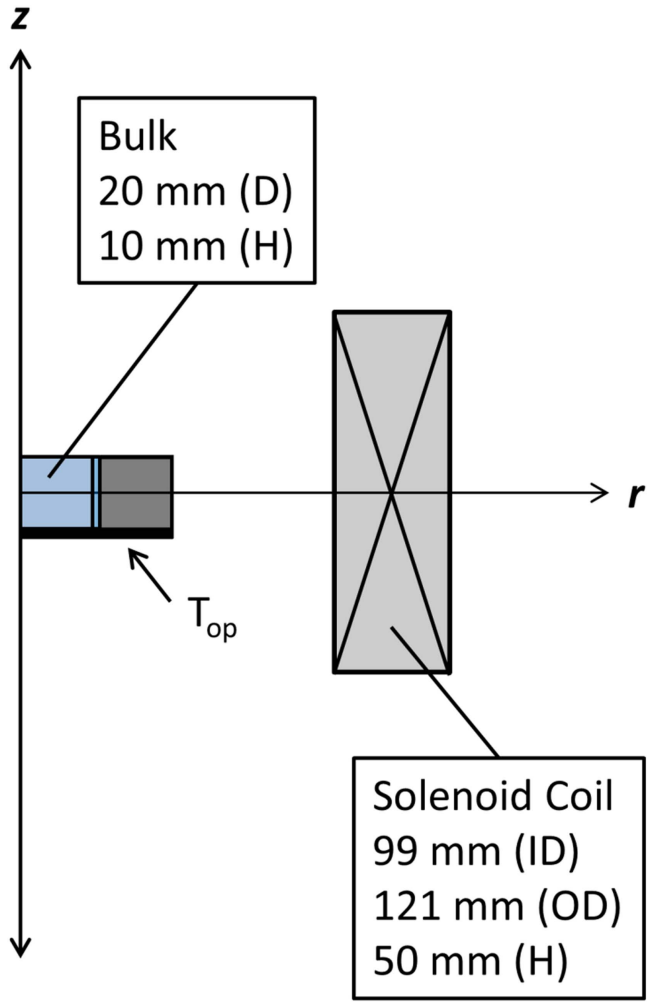

Figure 3. 2D axisymmetric model setup for numerical simulation of pulsed field magnetisation using a solenoid coil. A thin (0.2 mm) indium sheet is placed between the bulk and cold stage to provide a good thermal contact. The bulk, which is 20 mm in diameter and of thickness 10 mm, is embedded in a 316 stainless steel (SUS) ring using Stycast™ (2850GT). T_{op} is the operating temperature of the cold head, and is assumed to be 40 K in the following simulations.

subdomain, as described in [26], such that

$$I_{\text{pulse}}(t) = N \cdot I_0 \frac{t}{\tau} \exp\left(1 - \frac{t}{\tau}\right), \tag{4}$$

where I_0 is the peak magnitude of the current flowing in each turn of the solenoid coil, N is the number of turns, and τ is the rise time of the pulse, where $\tau = 15$ ms is assumed for each pulse. This setup has the same coil constant, relating B_{app} (the field at the centre of the magnetising fixture with the bulk removed) to $N \cdot I_0$ in equation (4), as presented in [26].

2.2. Simulation results

Firstly, we examine the effect of the magnitude of J_c on the simulated trapped field at the centre of the top surface of the bulk ($z = 0.1$ mm) at $T_{op} = 40$ K. Four samples of varying J_c are studied, with the $J_c(B, T)$ characteristics of the representative Ag-containing GdBCO sample divided or multiplied by an integer value, which varies the magnitude of J_c, but maintains the overall pinning characteristics of the sample [22].

- Low J_c $J_c(B, T)/3$
- Normal J_c $J_c(B, T)$
- High J_c $2J_c(B, T)$
- Ultra-high J_c $3J_c(B, T)$

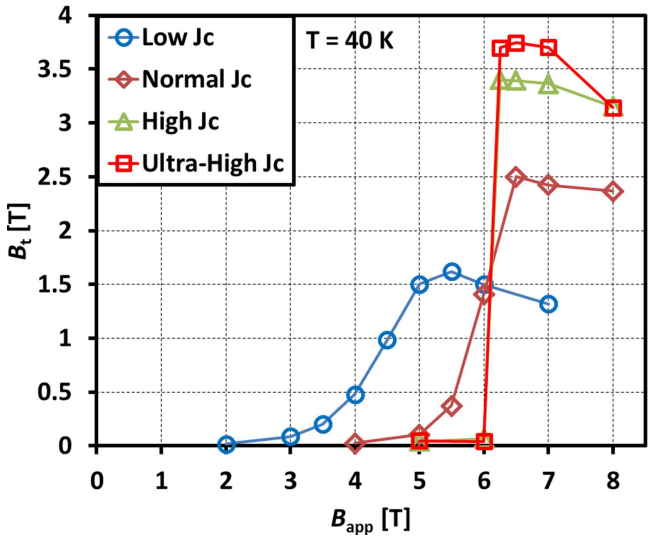

Figure 4. Numerical simulation results for the trapped magnetic field, B_t, at the centre of the top surface of the bulk samples ($r = 0$ mm) at a height of $z = 0.1$ mm at $t = 300$ ms for applied fields, B_{app}, up to 8 T and at an operating temperature, T_{op}, of 40 K.

Figure 4 shows a comparison of the trapped field, B_t, at the centre of the top surface of the bulk samples ($r = 0$ mm) at a height of $z = 0.1$ mm at $t = 300$ ms for applied fields, B_{app}, up to 8 T and at an operating temperature, T_{op}, of 40 K.

For the high J_c and ultra-high J_c samples, there is a large increase in the trapped field at the centre of the top surface for a relatively small increase in applied field (0.25 T) above 6 T, which is qualitatively consistent with the experimental results observed in [7, 18, 23–26]. For the high J_c sample, for example, B_t is close to zero when $B_{app} = 6$ T, but increases to 3.4 T when B_{app} is increased by 0.25 to 6.25 T. For increasing B_{app} values after the sample is fully magnetised, the trapped field begins to reduce due to an increasing temperature rise generated by the rapid movement of flux lines in the sample [29].

It was observed in [24] that standard YBCO samples of a similar size to this simulated bulk, with average, in-field J_cs of 10 kA cm^{-2} and $B_{t,max} = 0.4$ T at 77 K, produced similar results to the simulated low and normal J_c cases, with good agreement with the CSM, as well as previously reported numerical simulation results by the authors [26, 29, 45]. However, high-J_c samples fabricated by the U/n method, which introduces improved broken-columnar pinning centres after a sample doped with a constant mass% of U is irradiated with thermal neutrons [24], exhibit average, in-field J_cs of 50 kA cm^{-2} and $B_{t,max} = 2$ T at 77 K, as well as such jumps ('giant field leaps') in the measured trapped field with only a small increase in the applied field [7, 24, 25].

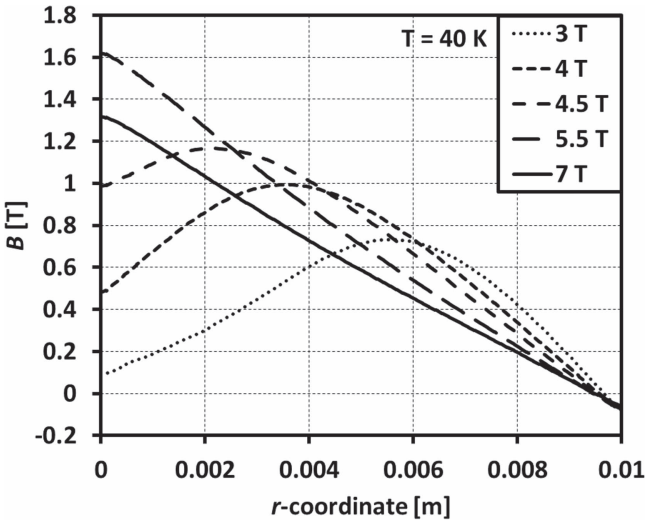

Figure 5. Numerical simulation results for the trapped magnetic field profile across the top surface of the low J_c sample ($z = 0.1$ mm) for increasing B_{app} between 3 and 7 T for $T_{op} = 40$ K. No flux jumps are observed.

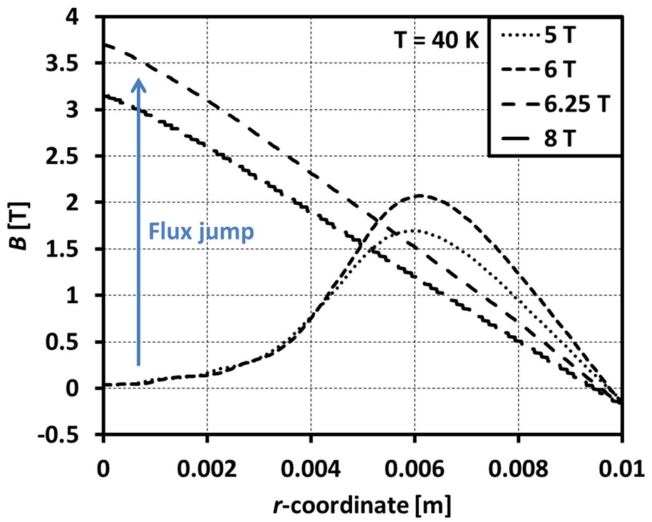

Figure 6. Numerical simulation results for the trapped magnetic field profile across the top surface of the high J_c sample ($z = 0.1$ mm) for increasing B_{app} between 5 and 8 T for $T_{op} = 40$ K. A large increase in the trapped field, due to flux jumps, is observed when increasing the applied field from 6 to 6.25 T.

It is also important to note that the maximum trapped field $B_t = 3.4$ T for $B_{app} = 6.25$ T for the high J_c sample is larger than the permissible value based on the simplistic CSM prediction, which suggests the field trapped at the centre is $\leqslant$ ½B_{app} for ZFC in the case of an infinitely long slab. Applying the Biot–Savart law to such a geometry, and assuming the CSM, would suggest that B_{app} should be 4 times the trapped field at the surface for full magnetisation of the superconductor. For this particular sample geometry, where the ratio of thickness/diameter is ½, an applied field of 3.276 times the surface trapped field would be required to fully magnetise the sample. This required applied field tends logarithmically to 2 times in the case of a thin sheet, where the central field can be assumed to be equal to the surface field. The same result is found for the ultra-high J_c sample, where $B_t = 3.7$ T for $B_{app} = 6.25$ T and $B_t = 3.75$ T for $B_{app} = 6.5$ T.

Furthermore, ordinarily for samples with increased J_c, the activation field (the applied pulsed field required to fully magnetise the sample [29]) also increases due to the stronger pinning forces that need to be overcome for the magnetic flux to fully penetrate the sample. In the case of the high and ultra-high J_c samples here, the flux jumps that occur act to reduce the activation field from its expected value, while allowing the sample to be fully magnetised with a high trapped field.

Figure 5 shows the numerical simulation results for the trapped magnetic field profile across the top surface of the low J_c sample ($z = 0.1$ mm) for increasing B_{app} between 3 and 7 T for $T_{op} = 40$ K. No flux jumps are observed, and the magnetic field penetration (and resultant trapped field) steadily increases with increasing B_{app}, until the sample is fully magnetised when $B_{app} = 5.5$ T. Further increases in B_{app} above this value results in full magnetisation, but a reduced maximum trapped field, consistent with previous experimental results observed by the authors [26, 29, 45], because of a larger temperature rise due to the higher applied field.

Figure 6 shows the same simulated trapped field profiles for the high J_c sample ($z = 0.1$ mm) for increasing B_{app} between 3 and 7 T for $T_{op} = 40$ K. As shown in figure 4, the trapped field profile suddenly changes between $B_{app} = 6$ and 6.25 T, to a conical (fully magnetised) trapped field profile from a peak-valley shape (partially magnetised), again qualitatively consistent with the experimental results presented in [7, 24, 25]. One obvious difference between those experimental results and these simulated results is the height of the peak in the partially magnetised state, which can be explained by the different magnetising fixture used: in [7, 24, 25], a split coil of smaller radius is used as the magnetising fixture, for which the magnetising mechanism is different in that, instead of flux penetrating from the periphery (or edge) of the bulk, the flux penetrates from the top/bottom surfaces [46, 47]; and the different operating temperature and pinning characteristics of the sample.

In order to study the magnetic flux dynamics in more detail, figure 7 shows the trapped field calculated at three discrete locations above the top surface of the bulk (again at $z = 0.1$ mm): centre, +4 mm, and +8 mm (2 mm from the edge of the 20 mm diameter sample). Figures 7(a)–(c) show the change in time of the field calculated at each point as the pulse is applied, then removed, for the low J_c sample for $B_{app} = 3$, 4.5, and 5 T, respectively. Again, these results are consistent with CSM predictions and the experimentally observed results in [7, 24, 25] for lower J_c, standard YBCO samples. The combination of a large applied field near the edge of the sample and the associated temperature rise due to the rapid movement of magnetic flux into the sample results in a localised, suppressed J_c, and the field at the +8 mm point from the centre almost follows the applied field for increasing B_{app} values. Figures 7(d)–(f) shows similar plots for the high J_c sample, where flux jumps act to assist the PFM process, resulting in a sudden, large increase in the trapped field at the

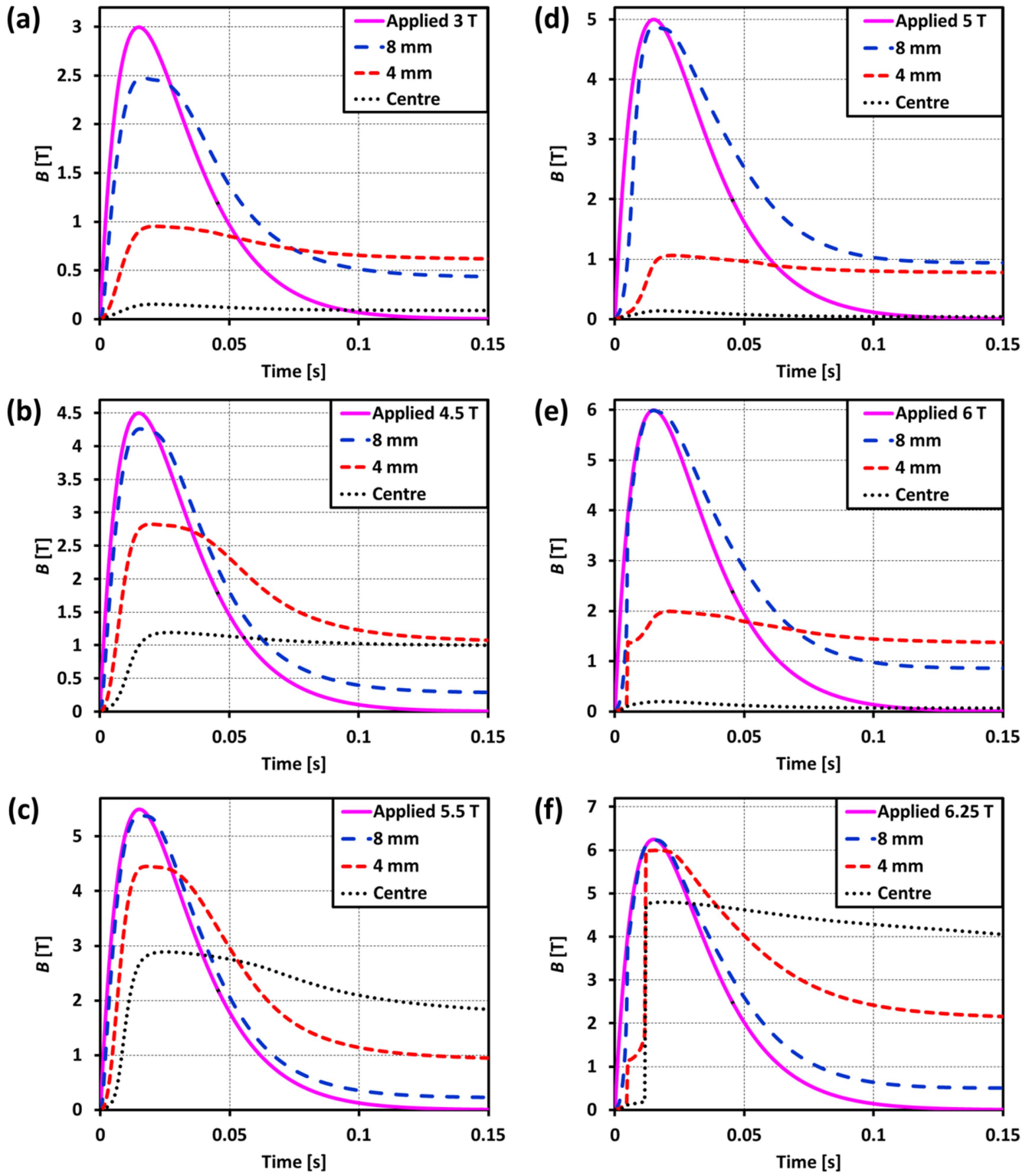

Figure 7. Trapped field calculated at three discrete locations above the top surface of the bulk ($z = 0.1$ mm): centre, +4 mm, and +8 mm (2 mm from the edge of the 20 mm diameter sample). Panels (a)–(c) show the change in time of the field calculated at each point for the low J_c sample for $B_{app} = 3$, 4.5, and 5 T, respectively. (d)–(f) show the change in time of the field calculated at each point for the high J_c sample for $B_{app} = 5$, 6, and 6.25 T, respectively.

centre of the sample. When $B_{app} = 5$ T, no flux jump is observed in the high J_c sample, and the magnetic flux dynamics are similar to those for the low J_c sample in figure 7(a). However, when $B_{app} = 6$ T, as shown in figure 7(e), a flux jump is observed at +4 mm between $t = 4.5$–5 ms, but there is no change at the centre of the sample. Increasing the applied field a further 0.25 T results in a second flux jump between $t = 11.5$–12 ms, as shown in

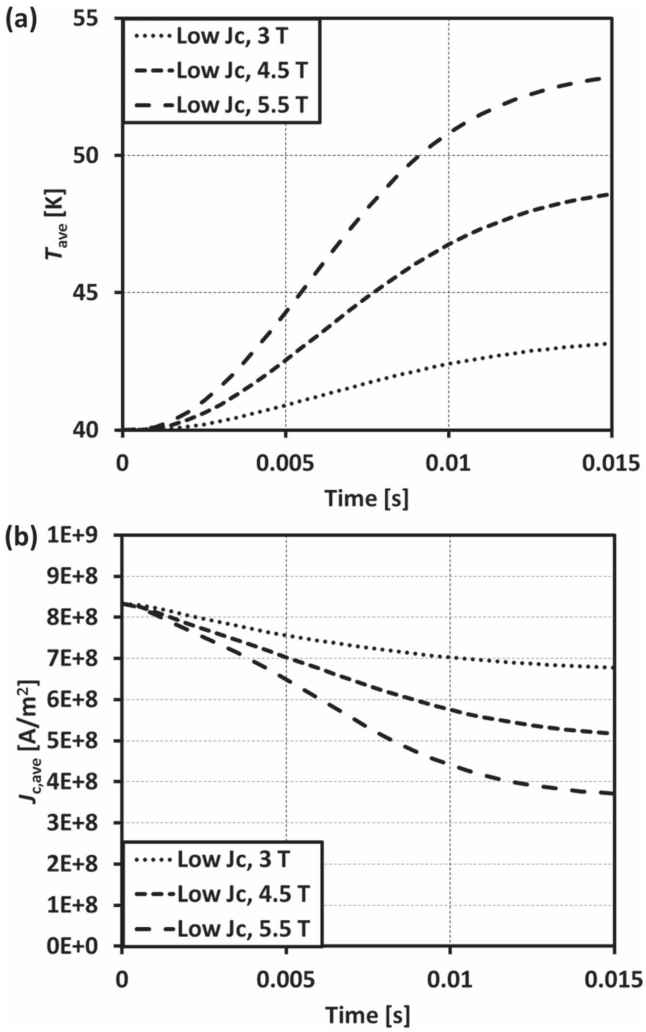

Figure 8. (a) Average temperature, T_{ave}, of the low J_c sample during the pulse, until the applied field reaches its peak value, for $B_{app} = 3$, 4.5 and 5.5 T. (b) The sample's average critical current density, $J_{c,ave}$, over the same period of time for the same applied fields.

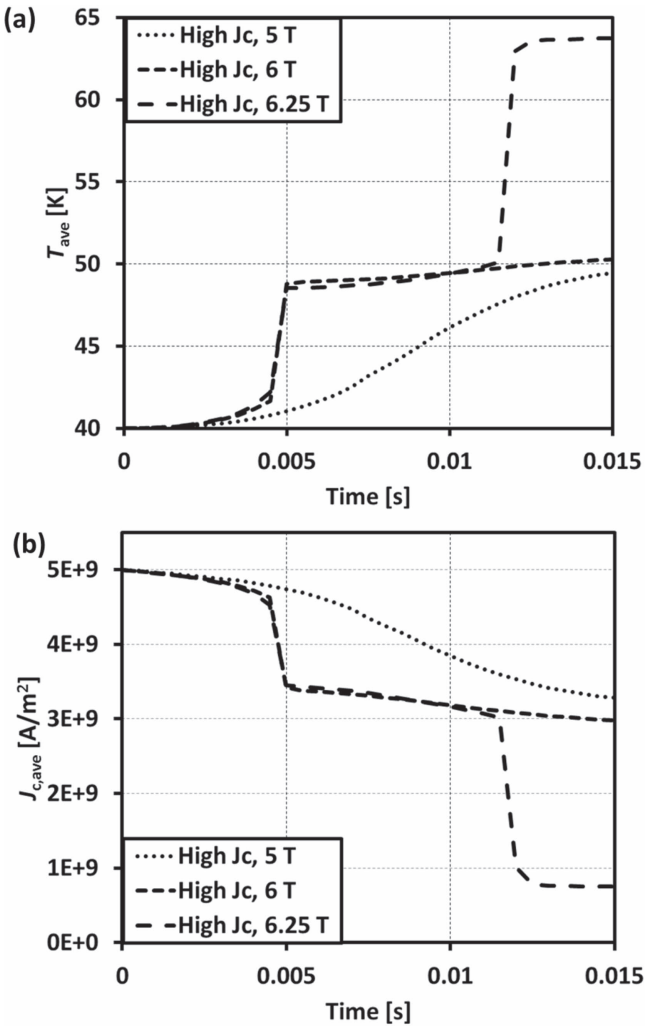

Figure 9. (a) Average temperature, T_{ave}, of the high J_c sample during the pulse, until the applied field reaches its peak value, for $B_{app} = 5$, 6 and 6.25 T. (b) The sample's average critical current density, $J_{c,ave}$, over the same period of time for the same applied fields.

figure 7(f). Consequently, a large and sudden increase in magnetic field is seen at the centre, resulting in full magnetisation of the sample.

Figure 8(a) shows the average temperature, T_{ave}, of the low J_c sample during the pulse until the applied field reaches its peak value and figure 8(b) shows the sample's average critical current density, $J_{c,ave}$. Both T_{ave} and $J_{c,ave}$ are calculated by integrating T and J_c, respectively, over the cross-sectional area of the bulk, and the result is divided by this area. There is a smooth increase in temperature and decrease in J_c due to the magnetic flux penetration during the rising pulse. Since the time constant, τ, of each pulse is the same, a higher B_{app} value results in higher dB/dt and larger field penetration, resulting in a larger temperature rise and further suppression of J_c. Figures 9(a) and (b) show the same plots for the high J_c sample. For $B_{app} = 5$ T for the high J_c sample, where no flux jump occurs, there is a similar smooth increase in T_{ave} and reduction in $J_{c,ave}$. The flux jumps that occur for higher applied fields, $B_{app} = 6$, 6.25 T, are accompanied by a large and sudden temperature rise and a simultaneous, mirrored reduction in $J_{c,ave}$. The temperature rise during PFM takes place adiabatically [3], because a large proportion of the heat generation takes place instantaneously and the cooling power is finitely limited. The low thermal conductivity of the bulk also seriously affects the thermal and electromagnetic responses, for which the thermal diffusion is much slower than the magnetic diffusion. When modelling typical experimental conditions, and for a typical rise time of $\tau \approx 10$ ms of the applied pulse, the magnetic flux propagation can be an order of magnitude or higher faster than the heat propagation [48]. Another example of such behaviour can be observed in figure 21 in [26].

In [24, 25], it was speculated that a large Lorentz force, given by $\boldsymbol{F}_L = \boldsymbol{J} \times \boldsymbol{B}$, acting on the magnetic flux penetrating the sample during the PFM process is a cause of the flux jumps into the sample. In order to clarify this hypothesis, figure 10 shows the calculated maximum Lorentz force density in each of the bulk samples, until the pulse reaches its peak value, for (a) $B_{app} = 5$ T, (b) $B_{app} = 6$ T, and (c) $B_{app} = 7$ T. Here, the Lorentz force density in the $-r$

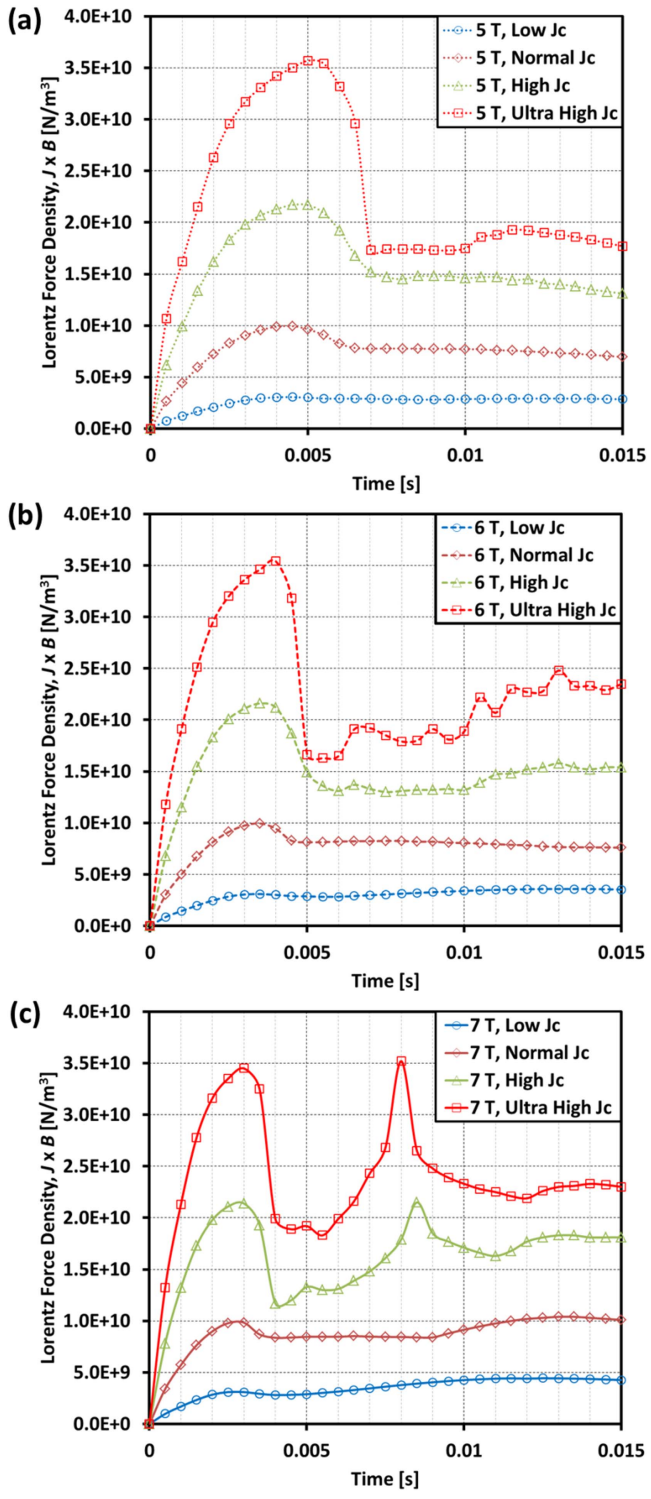

Figure 10. Calculated maximum Lorentz force density, $\boldsymbol{J} \times \boldsymbol{B}$, in the $-r$ direction in the bulk samples, until the pulse reaches its peak value, for (a) $B_{\text{app}} = 5$ T, (b) $B_{\text{app}} = 6$ T, and (c) $B_{\text{app}} = 7$ T.

direction is calculated, which drives the magnetic flux towards the centre of the sample, and is given by $-J_{\phi}\mu_0 H_z$. For $B_{\text{app}} = 5$ T, no flux jumps occur for the low, normal and high J_c samples, but there is a flux jump between $t = 6.5$–7 ms for the ultra-high J_c sample. As shown in figure 10(a), the maximum Lorentz force density in the sample increases with J_c, and the flux jump in the ultra-high J_c sample is preceded firstly by a large F_L, followed by a slight reduction in F_L, which rapidly reduces when the flux jump occurs. When B_{app} is increased to 6 T, as shown in figure 10(b), this behaviour becomes more pronounced. Finally, when B_{app} is increased to 7 T, as shown in figure 10(c), two flux jumps are observed for the high and ultra-high J_c samples, with the latter one causing flux to jump all the way into the centre of the sample. This secondary flux jump is preceded by the attainment of a large F_L value, comparable to the F_L value at which the first flux jump occurred. These results provide good evidence that the flux leap in high-J_c bulk superconductors is due to the large Lorentz force acting on the magnetic flux penetrating the sample, which causes flux to jump further into the sample, resulting in a sudden and large increase in temperature and reduction in J_c (as shown in figure 9). The maximum value of J/J_c during the pulse rise time was also examined to discern whether this is a cause of the flux jumps, and no correlation between J/J_c and the flux jumps was observed. In fact, in the case of the normal J_c bulk, J/J_c exceeded 2 during the pulse rise time for $B_{\text{app}} = 6$, 7 T, for example, with no flux jumps observed.

Hence, if the F_L value is large enough, a flux jump to the centre of the sample can be induced that can fully magnetise a sample, with a reduction in the required activation field, which is significant for practical applications as such flux jumps could be exploited to provide higher trapped fields, whilst reducing the cost and size of the magnetising fixture. This numerical simulation framework provides a flexible and cost-effective method for analysing and optimising different magnetising fixtures, as well as examining the effect of different J_c and pinning characteristics of other families of superconducting materials and/or materials made from different processing techniques.

3. Conclusion

So-called 'giant field leaps' have been observed by a number of research groups investigating PFM of bulk high-temperature superconductor, where flux jumps occur in the superconductor, and magnetic flux suddenly intrudes into the centre of the sample. This phenomenon is assistive to the PFM process and results in a large increase in the measured trapped field at the centre of the top surface and full magnetisation of the sample. In this paper, a 2D axisymmetric finite-element model implementing the $\boldsymbol{H}$-formulation, with a modified E–J power law characteristic representing the normal state resistivity of the superconductor when $J > J_c$, is used to qualitatively reproduce this phenomenon to good effect. By simply inserting a bulk sample of high J_c, as found in high quality standard samples and neutron-irradiated ones, such 'giant field leaps' or flux jumps are observed in the model, due to the large Lorentz force, F_L, generated during the PFM process that drives the magnetic flux into the sample. The flux jumps are accompanied by a large and sudden temperature rise, and a simultaneous, mirrored reduction in

$J_{c,ave}$. The maximum value of J/J_c during the pulse rise time was also examined to discern whether this is a cause of the flux jumps, and no correlation between J/J_c and the flux jumps was observed. The numerical simulation framework is extremely flexible and provides a cost-effective method for analysing and optimising different magnetising fixtures, as well as examining the effect on samples of different J_c and pinning characteristics, to exploit such flux jumps to enhance the trapped field in practical, bulk superconductor applications.

Acknowledgments

Dr Mark Ainslie would like to acknowledge the support of a Royal Academy of Engineering Research Fellowship. The authors would like to thank Archie Campbell, University of Cambridge, for his useful discussions.

References

[1] Tomita M and Murakami M 2003 *Nature* **421** 517–20
[2] Durrell J H *et al* 2014 *Supercond. Sci. Technol.* **27** 082001
[3] Ainslie M D and Fujishiro H 2015 *Supercond. Sci. Technol.* **28** 053002
[4] Nariki S, Sakai N and Murakami M 2005 *Supercond. Sci. Technol.* **18** S126–30
[5] Weinstein R, Sawh R-P, Parks D and Mayes B 2012 *Nucl. Instrum. Meth.* B **272** 284–90
[6] Weinstein R *et al* 2000 *Physica* C **341–348** 1415–8
[7] Weinstein R *et al* 2015 *IEEE Trans. Appl. Supercond.* **25-3** 6601106
[8] Hull J and Murakami M 2004 *Proc. IEEE* **92** 1705–18
[9] Murakami M 2007 *Int. J. Appl. Ceram. Technol.* **4** 225–41
[10] Zhou D *et al* 2012 *Supercond. Sci. Technol.* **25** 103001
[11] Zhang Y *et al* 2016 *Supercond. Sci. Technol.* **29** 044005
[12] Yokoyama K *et al* 2003 *IEEE Trans. Appl. Supercond.* **13-2** 1592–5
[13] Nakamura T *et al* 2007 *Concepts Magn. Reson.* B **31B** 65
[14] Nakamura T *et al* 2015 *J. Magn. Reson.* **259** 68–75
[15] Fujishiro H, Itoh Y, Yanagi Y and Nakamura T 2015 *Supercond. Sci. Technol.* **28** 095018
[16] Saho N *et al* 2009 *Physica* C **469** 1286–9
[17] Nishijima S *et al* 2009 *IEEE Trans. Appl. Supercond.* **19-3** 2257–60
[18] Fujishiro H *et al* 2005 *Physica* C **445–448** 334–8
[19] Itoh Y and Mizutani U 1997 *Japan. J. Appl. Phys.* **35** 2114–25
[20] Itoh Y, Yanagi Y and Mizutani U 1997 *J. Appl. Phys.* **82** 5600–11
[21] Ikuta H *et al* 2002 *Supercond. Sci. Technol.* **15** 606–12
[22] Mizutani U *et al* 1998 *Appl. Supercond.* **6** 235–46
[23] Yanagi Y *et al* 2005 *Supercond. Sci. Technol.* **18** 839–49
[24] Weinstein R *et al* 2015 *Appl. Phys. Lett.* **107** 152601
[25] Weinstein R *et al* 2016 *J. Appl. Phys.* **119** 133906
[26] Ainslie M D *et al* 2016 *Supercond. Sci. Technol.* **29** 074003
[27] Cha Y S 2005 *Chin. J. Phys.* **43** 681–92 (http://psroc.org/cjp/download.php?type=paper&vol=43&num=3-II&page=681)
[28] COMSOL, Inc. (www.comsol.com)
[29] Ainslie M D *et al* 2014 *Supercond. Sci. Technol.* **27** 065008
[30] Plummer C J G and Evetts J E 1987 *IEEE Trans. Magn.* **23** 1179–82
[31] Rhyner J 1993 *Physica* C **212** 292–300
[32] Duron J *et al* 2004 *Physica* C **401** 231–5
[33] Duron J *et al* 2007 *Supercond. Sci. Technol.* **20** 338–44
[34] Xia J and Zhou Y 2015 *Cryogenics* **69** 1–9
[35] Zou J *et al* 2015 *Supercond. Sci. Technol.* **28** 075009
[36] Zou S, Zermeno V M R and Grilli F 2016 *IEEE Trans. Appl. Supercond.* **26** 4702405
[37] Brandt E H 1995 *Rep. Prog. Phys.* **58** 1465–594
[38] Hu D *et al* 2015 *Supercond. Sci. Technol.* **28** 065011
[39] Hu D *et al* 2016 *IEEE Trans. Appl. Supercond.* **26** 6600906
[40] Jirsa M, Půst L, Dlouhý D and Koblischka M R 1997 *Phys. Rev.* B **55** 3276–84
[41] Fujiyama K, Shiraishi R and Ohsaki H 2005 *Physica* C **426–431** 681–7
[42] Shiraishi R and Ohsaki H 2006 *IEEE Trans. Appl. Supercond.* **16** 1794–7
[43] Zhang M, Matsuda K and Coombs T A 2012 *J. Appl. Phys.* **112** 043912
[44] Fujishiro H *et al* 2011 *Supercond. Sci. Technol.* **24** 105003
[45] Ainslie M D *et al* 2015 *Supercond. Sci. Technol.* **28** 125002
[46] Xu Z *et al* 2012 *Supercond. Sci. Technol.* **25** 025016
[47] Fujishiro H, Naito T and Oyama M 2011 *Supercond. Sci. Technol.* **24** 075015
[48] Fujishiro H and Naito T 2010 *Supercond. Sci. Technol.* **23** 105021